CONF-810804--24

MASTER

NONEQUILIBRIUM FLASHING MODEL FOR RAPID PRESSURE TRANSIENTS

CONF-810804--24

DE82 007639

F. Aguilar
Manager, Code Development Division
EG&G Idaho
Idaho Falls, ID 83415
Member ASME

S. Thompson
Senior Mathematician
Babcock and Wilcox Company
Lynchburg, VA 24505

NOTICE

This report was prepared as an account of work sponsored by an agency of the United States Government. Neither the United States Government nor any agency thereof, or any of their employees, makes any warranty, expressed or implied, or assumes any legal liability or responsibility for any third party's use, or the results of such use, of any information, apparatus, product or process disclosed in this report, or represents that its use by such third party would not infringe privately owned rights. The views expressed in this paper are not necessarily those of the U.S. Nuclear Regulatory Commission.

Work supported by the U.S. Nuclear Regulatory Commission, Office of Nuclear Regulatory Research under DOE Contract No. DE-AC07-76ID01570.

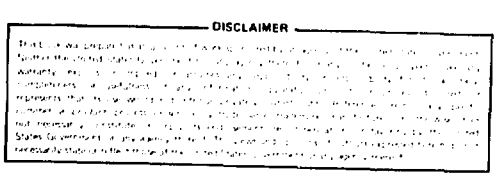

ABSTRACT

A detailed, microscopic model for the nonequilibrium flashing of water is coupled tc equations describing the bulk liquid state in order to calculate rapid pressure response to an induced liquid strain. The flashing model is predicated on the dynamics of a single bubble growing in an infinite liquid, and it encompasses both the inertia and conduction-limited regimes of bubble growth. The analysis is valid at high temperatures. It is not limited by the assumption of a thin thermal boundary layer for the bubble or by a prescribed boundary layer shape. The analysis can predict arbitrary pressure transients, both decompressive and recompressive.

The flashing model involves the solution of a system of ordinary and partial differential equations constituting a classic moving-boundary problem. The solution is obtained numerically by the method of lines and by the use of automatic software.

The chamber-and-piston experiment of Friz et al. [4] is analyzed, and the pressure response of the system is studied for various combinations of two input parameters, bulk nucleation superheat and nucleation site density. It appears that more than one combination of these parameters can produce an adequate fit to the experimental data. It is demonstrated that bulk nucleation can take place long before the maximum liquid superheat is attained. The parametric study underscores the difficulty of inferring the onset of homogeneous nucleation from pressure-time data alone. It also confirms that constant superheat theory does not adequately predict nonequilibrium flashing in rapid pressure transients.

NOMENCLATURE

a	Sound Speed
E	Internal Energy
h	Specific Enthalpy
Ja	Jakob Number
k_f	Liquid Thermal Conductivity
M	Mass
N	Nucleation Site Density
P	Pressure
P_b	Bubble Vapor Pressure
P_∞	Macroscopic Liquid Pressure
Pr	Prandtl Number
r_b	Dimensionless Bubble Radius, Equation (6)
R	Radial Spherical Coordinate
R_b	Bubble Radius
R_{bo}	Initial, Critical Bubble Radius
t	Time
T	Temperature
T_L	Interface Temperature
T_s	Saturation Temperature
T_∞	Macroscopic Liquid Temperature
ΔT	Liquid Superheat, $T_\infty - T_s(P_\infty)$
y	Dimensionless Distance from Bubble Surface, Equation (4a)
V	Volume
ΔV	Piston Displacement
ϵ	Density Parameter, $(\rho_f - \rho_g)/\rho_f$
ρ_f	Liquid Density
ρ_g	Saturated Vapor Density
ν_f	Liquid Kinematic Viscosity
σ	Surface Tension
θ	Dimensionless Temperature Defect, Equation (5)
τ	Dimensionless Time, Equation (46)

INTRODUCTION

Interest in the problem of homogeneous nucleation and flashing in a superheated liquid undergoing rapid decompression has been spurred by nuclear reactor safety considerations. The nearly instantaneous, guillotine rupture of a coolant pipe in a pressurized water reactor (PWR) is a design constraint for reactor vessel internal structures and supports. Upon such a loss-of-coolant accident, a train of decompression waves would propagate into the subcooled reactor system and load various structures. Because of the very rapid blowdown rates postulated (on the order of 1-10 MPa/ms), it is conceivable that the reactor coolant could become highly superheated before flashing.

Pressure undershoots below saturation values have been observed in a number of blowdown experiments [1,2,3] including Friz, et al. [4]. Recently Lienhard, et al. [5] studied the extremely rapid blowdown of subcooled water within a pipe equipped with a novel quick-opening mechanism. They found the magnitude of pressure undershoot to be dependent on blowdown rate. For thermodynamic states typical of PWR operation, the maximum pressure undershoot was observed to approach a limit as blowdown rate was increased. The limiting value of liquid superheat was approximately 65% of the spinodal limit.

This paper presents a general solution technique that is the first step toward the capability to analyze separate effects experiments like Lienhard's and toward the inclusion of nonequilibrium flashing effects in the calculation of reactor loadings. The analysis is predicated on the dynamics of a single bubble growing in an infinite liquid. The conduction equation for the thermal layer enveloping the bubble is solved together with the bubble mass and motion equations. This system of partial and ordinary differential equations describes a classic moving-boundary or Stefan problem, and the somewhat novel solution presented here is of interest of itself. The solution is compared with Niino's [6,7] bubble growth measurements in a decreasing pressure field.

However, the microscopic equations for bubble growth are also coupled to macroscopic equations describing the bulk liquid state. The idea is to illustrate how the feedback between the flashing process and an induced liquid strain can be handled to calculate pressure response given the number of nucleation sites and the nucleation superheat. It is assumed that nucleation occurs simultaneously at all sites, and these are dispersed uniformly throughout the liquid. The chamber-and-piston experiment of Friz, et al. [4] is analyzed in this manner for varied combinations of nucleation superheat and nucleation site density. This analysis addresses the question of whether homogeneous nucleation occurs at the time of "turn around" of an experimental pressure-time trace or before.

The solution technique described in this paper uses some methods which have not as yet received widespread attention in the engineering literature. The moving boundary is first made stationary by a transformation of variable. The coupled system of partial and ordinary differential equations is then solved numerically by finite differences, specifically by the method of lines. An automatic solver is used to integrate the resulting system of ordinary differential equations. The Keenan, et al. [8] fundamental equation for water is used to evaluate both stable and metastable thermodynamic states. It is anticipated that the present analysis will provide an interesting example of how these powerful tools can be readily used to solve similar engineering problems.

ANALYSIS

The description of bubble growth on a microscopic scale is central to the analysis presented here. This is a familiar problem, which Besant [9] first investigated over one hundred years ago. Rayleigh's [10] simpler derivation for bubble collapse in an infinite, incompressible liquid extends the solution to permit variation in bubble pressure. However, the Rayleigh solution has two limitations. It is derived on the assumption that the liquid pressure is held constant away from the bubble, and it is

applicable only in the range of high Jakob numbers, i.e., the range where bubble growth is limited by the inertia of the surrounding liquid and not by the mass transfer rate at the bubble surface.

The approximate solutions of Plesset and Zwick [11], Forster and Zuber [12], and Scriven [13] treat the case where bubble growth is limited by interfacial mass transfer, which is controlled by heat conduction through the bubble thermal layer. These solutions are obtained for constant pressure, and are in essential agreement--the bubble radius grows at $t^{1/2}$. A simple general relation spanning both the inertia and conduction controlled regions has been derived by Mikic et al. [14] for the constant pressure case.

Jones and Zuber [15] have demonstrated that the constant pressure theory of conduction-limited growth fails when applied to a transient pressure field. For example, the bubble radius grows as $t^{n+1/2}$ for decompression transients during which the saturation temperature of the liquid varies at t^n. The Jones and Zuber solution is obtained in integral form and describes conduction-controlled growth only. It is restricted by the assumption of a thin thermal layer, and it is not applicable to arbitrary pressure transients composed of both decompressive and recompressive events.

A numerical solution for bubble growth in a transient pressure field has been obtained by Theofanous et al. [16]. The analysis accounts for the effects of both liquid inertia and conduction in the thermal layer. Nonequilibrium vaporization at the bubble surface is considered as well. Theofanous et al. treat the thermal layer by assuming a quadratic temperature distribution as in the method of Bornhorst and Hatsopoulos [17]. The partial differential equation describing the thermal layer is integrated from the bubble surface to the edge of the thermal layer. This reduces the conduction equation to an ordinary differential equation with respect to time but introduces the thermal layer thickness as an unknown. Bornhorst and Hatsopoulos obtain closure by restricting their

analysis to very thin layers. Theofanous, et al. obtain closure by substituting the quadratic temperature profile into a boundary condition coupling heat and mass fluxes at the bubble surface. This equation is then differentiated with respect to time to obtain an expression for the time derivative of the thermal layer thickness.

The above analyses may be distinguished according to how the thermal layer is treated. The assumptions made in handling the thermal layer often prove to be the ones that narrow the applicability of a solution. The analysis presented below offers a more rigorous and less restrictive treatment of the thermal layer as no assumptions are made regarding the thermal layer thickness or shape. This is essential, because the model is required to handle the arbitrary pressure transients, both decompressive and recompressive, that result from wave action during blowdown of a PWR.

The present analysis is general in other aspects as well. Obviously, the flashing model must be applicable at the high pressures and temperatures of PWR operation. It must also handle the severe superheats observed by Lienhard, et al. for rapid decompression. Consequently, the density parameter ϵ is not assumed to be close to 1 nor constant. Water vapor is not treated as an ideal gas. Finally, the analysis can describe both inertia and mass transfer controlled growth.

Governing Equations

The microscopic flashing model is described first. The macroscopic equations describing the bulk liquid state are then derived for a prescribed liquid strain. Finally, the equation sets are coupled to determine pressure response.

Conservation of mass for a liquid system bounded by concentric spheres of radii R_b (the bubble surface) and R yields

$$u(R,t) = \frac{1}{3R^2}\frac{d}{dt}\left[\epsilon R_b^3\right], \quad R > R_b \tag{1}$$

It is assumed that the liquid is incompressible and that individual bubbles are sparsely distributed within the liquid. Substitution of Equation (1) into the momentum equation for spherically symmetric flow (see [17]) results in

$$\frac{d^2}{dt^2}\left[\epsilon R_b^3\right] + \left\{\frac{4\nu_f}{R_b^2} - \frac{1}{6R_b^3}\frac{d}{dt}\left[\epsilon R_b^3\right]\right\}\frac{d}{dt}\left[\epsilon R_b^3\right]$$

$$= \frac{3\left[P_b - P_\infty\right]}{\rho_f}\left\{R_b - \frac{2\sigma}{P_b - P_\infty}\right\} \tag{2}$$

Equation (2) determines bubble growth given the bubble pressure P_b and the pressure P_∞ of the liquid. The bubble pressure is in turn governed by the bubble growth rate and the interfacial heat and mass transfer rates. It is assumed here that the vapor is in thermodynamic equilibrium with the surrounding liquid. Thus the bubble pressure P_b is simply the saturation pressure corresponding to the interface temperature. Nonequilibrium at the bubble interface is not considered here, because the results of [17] indicate that nonequilibrium effects are not particularly significant at the high temperatures of PWR operation. However, such effects can easily be incorporated into the analysis as will be evident below.

Therefore if the liquid pressure is known with time, problem closure only requires the calculation of the liquid temperature and temperature

gradient at the bubble surface. These are given by the solution of the energy equation:

$$\frac{\partial T}{\partial t} + u \frac{\partial T}{\partial R} = \frac{\alpha}{R^2} \frac{\partial}{\partial R} \left[R^2 \frac{\partial T}{\partial R}\right] \tag{3a}$$

in which the liquid thermal diffusivity is assumed constant. The auxiliary conditions are:

$$T(R,0) = T_\infty \text{ (constant)}, \quad R_b < R < \infty \tag{3b}$$

$$\lim_{R \to \infty} T(R,t) = T_\infty \quad , \quad t \geq 0 \tag{3c}$$

$$\frac{\partial T}{\partial R}(0,t) = \frac{h_{fg} \rho_f}{3k_f R_b^2} \frac{d}{dt} \left[(1-\varepsilon) R_b^3\right], \quad t \geq 0 \tag{3d}$$

Conditions (3b) and (3c) indicate that there are no initial temperature gradients within the liquid and that the blowdown proceeds isothermally. This, of course, is not strictly true. Equation (3d) results from treating the bubble surface as an open system and applying the first law. It is assumed that the interface is in thermal equilibrium and that changes in film energy are negligible.

The difficulty in obtaining the solution of Equation (3) is that the domain of the partial differential equation is not stationary. The motion of the boundary R_b is given by Equation (2), which is coupled to the solution of Equation (3) itself. The first step is to introduce the transformation of variable

$$y = \left[R - R_b\right] \left[\alpha t\right]^{-1/2} \tag{4a}$$

$$\tau = \alpha t / R_{bo}^2 \tag{4b}$$

The variable y is the distance from the bubble surface made dimensionless by an approximate thermal layer thickness. It is also convenient to define the temperature defect θ as

$$\theta = \left[T_\infty - T\right] / \left[T_\infty - T_s(P_\infty)\right] = \left[T_\infty - T\right] / \Delta T \tag{5}$$

and to scale the bubble radius with its initial value

$$r_b = R_b / R_{bo} \tag{6}$$

Combining Equations (1) through (6) results in the microscopic flashing model:

$$\frac{d^2}{d\tau^2}\left[\epsilon r_b^3\right] + \frac{1}{r_b^2}\left\{4Pr - \frac{1}{6r_b}\frac{d}{d\tau}\left[\epsilon r_b^3\right]\right\}\frac{d}{d\tau}\left[\epsilon r_b^3\right]$$

$$= \frac{3 R_{bo}^2 \left[P_b - P_\infty\right]}{\rho_f a^2}\left\{r_b - \frac{2\sigma}{R_{bo}\left[P_b - P_\infty\right]}\right\} \tag{7}$$

$$\frac{\partial\theta}{\partial\tau} = \left[\tau Z\right]^{-1}\frac{\partial}{\partial y}\left[Z\frac{\partial\theta}{\partial y}\right] + \tau^{-1/2}\left[\frac{dr_b}{d\tau} + \frac{1}{2}y\tau^{-1/2} - \frac{1}{3Z}\frac{d}{d\tau}\left[\epsilon r_b^3\right]\right]\frac{\partial\theta}{\partial y}$$

$$+ \frac{1}{\Delta T}\frac{dT_s}{dP}(P_\infty)\frac{dP_\infty}{d\tau}\theta \tag{8}$$

where

$$Z = \left[r_b + y\tau^{1/2}\right]^2.$$

The auxiliary data for the flashing model are

$$\left(\varepsilon r_b^3\right) = \left[\rho_f - \rho_g(T_i)\right] / \rho_f, \quad \tau = 0 \tag{9a}$$

$$\frac{d}{d\tau}\left[\varepsilon r_b^3\right] = 0, \quad \tau = 0 \tag{9b}$$

$$\theta(y,0) = 0, \quad 0 < y < \infty \tag{9c}$$

$$\lim_{y\to\infty} \theta(y,\tau) = 0, \quad \tau > 0 \tag{9d}$$

$$\frac{\partial\theta}{\partial y}(0,\tau) = -\frac{\tau^{1/2}}{3Ja\ (1-\varepsilon) r_b^2}\frac{d}{d\tau}\left[(1-\varepsilon) r_b^3\right], \quad \tau > 0 \tag{9e}$$

and

$$P_b = P_s(\theta_i), \quad \frac{dTs}{dP} = f_s(P_\infty), \text{ and } Ja = g_s(\theta_i)\ . \tag{9f}$$

There are a number of things to note about the flashing model. First, the bubble begins growth from a state of metastable equilibrium with the initial radius $R_{bo} = 2\sigma / \left[P_b - P_\infty\right]$. If the liquid pressure is held constant, the bubble cannot grow. The system must be perturbed. Second, in the limit of large Jakob numbers, condition (9e) reduces to $\partial\theta/\partial y = 0$ and the energy equation has the solution $\theta(y,\tau) = 0$. This implies that $P_b = P_s(T_\infty)$ for all time and that Equation (8) controls growth. This is Rayleigh or inertia limited growth. Third, the time derivative of the bulk liquid pressure appears explicitly in the energy equation. Its coefficient is evaluated at P_∞ with the Clapeyron equation

$$\frac{dT_s}{dP} = \frac{\dot{n}_{fg}}{T_s v_{fg}}$$

The apparent mathematical eccentricities of the model should be noted as well. The temperature defect θ assumes an indeterminate form in the limit as $T_s(P_\infty)$ approaches T_∞, i.e., as the liquid recovers from its superheated state to equilibrium. The temperature defect does remain finite upon recovery, and no adverse consequences have been encountered. Also, the transformed energy equation is singular at $\tau = 0$ as can be inferred from the definition of the distance y. It can be shown that

$$\lim_{\tau \to 0} \partial\theta/\partial\tau = 0,$$

and thus the singularity is removable. The singularity causes no unusual computational difficulties.

The objective now is to couple the mechanistic flashing model described above to equations describing the macroscopic liquid state in order to predict the pressure response of the bulk liquid. It is assumed that the external strain imposed on the liquid is a known function of time. This is the situation in the chamber and piston experiment of Friz, et al. [4] in which the piston displacement is measured with time. The more general case--actually the next step beyond the present analysis--is to incorporate the liquid motion equation.

This present limitation is not serious. On the contrary, the Friz experiment has great potential value precisely because the system is closed and the liquid strain is controlled. The calculation of the liquid strain within an open system is encumbered by the additional problem of determining the discharge flow. Thus, the present analysis focuses on the isolated interaction of bubbles and pressure field.

We consider then a system of subcooled liquid having an initial volume V_1, suddenly expanded at time τ_i according to $\Delta V(t) > 0$. The system path crosses the saturation line at time τ_2 without flashing. When the liquid superheat reaches a prescribed value at τ_3, nucleation occurs simultaneously at NV_1 sites dispersed uniformly throughout the system.

The liquid pressure is determined by two independent system properties. The liquid density is evaluated from the rates of change of the volume and mass which are available from the imposed displacement and the solution of Equations (7), (8), (9):

$$\frac{dV}{d\tau} = \begin{cases} \frac{d}{d\tau}[\Delta V] & , \tau \leq \tau_3 \\ \frac{d}{d\tau}[\Delta V] - \frac{4\pi N R_{bo}^3 V_1}{3} \frac{d}{d\tau}\left[r_b^3\right] & , \tau > \tau_3 \end{cases} \tag{11}$$

$$\frac{dM}{d\tau} = \begin{cases} 0 & , \tau \leq \tau_3 \\ \frac{4\pi N R_{bo}^3 M_1}{3} \frac{d}{d\tau}\left[\frac{\rho_g(T_i)}{\rho_1} r_b^3\right] & , \tau > \tau_3 \end{cases} \tag{12}$$

A first law analysis of the open system encompassing the liquid and the liquid-vapor interface gives a second independent property:

$$\frac{dE}{d\tau} = \begin{cases} -P \frac{d}{d\tau}[\Delta V] & , \tau \leq \tau_3 \\ -\left\{P \frac{d}{d\tau}[\Delta V] - \frac{4\pi N R_{bo}^3 V_1}{3} P_s(T_i) \frac{d}{d\tau}\left[r_b^3\right]\right\} & \\ -h_g(T_i) \frac{4\pi N R_{bo}^3}{3} V_i \frac{d}{d\tau}\left[\rho_g(T_i) r_b^3\right] & , \tau > \tau_3 \end{cases} \tag{13}$$

Equations (11), (12), and (13) define the liquid state. However, two additional expressions obtained with the chain rule are carried along as well:

$$\frac{dT}{d\tau} = \left.\frac{\partial T}{\partial e}\right|_\rho \frac{d}{d\tau}(E/M) + \left.\frac{\partial T}{\partial \rho}\right|_e \frac{d}{d\tau}(M/V) \tag{14}$$

and

$$\frac{dP}{d\tau} = \left.\frac{\partial P}{\partial T}\right|_{\rho} \frac{dT}{d\tau} + \left.\frac{\partial P}{\partial \rho}\right|_{T} \frac{d}{d\tau}\,(M/V) \qquad (15)$$

The temperature expression, Equation (14), is introduced so that the Keenan, et al. [8,18] fundamental equation can be used explicitly to evaluate the liquid state. The fundamental equation, which gives the Helmholtz energy as a function of density and temperature, possesses a number of attractive features. It is everywhere smooth (differentiable), and represents a continuum of single phase states through both the liquid and vapor regions. A subcritical isotherm plotted on the P-ρ plane resembles Van der Waals'. The Keenan equation is used here in an extrapolative sense to evaluate metastable liquid states. With the Keenan formulation, all thermodynamic properties can be evaluated for very nearly the same effort required to evaluate one. In the present case, the specific internal energy, entropy, pressure, and the four property derivatives imbedded in Equations (14) and (15) are evaluated virtually simultaneously given a density-temperature pair.

Equation (15) can be eliminated by substitution into Equation (8). It is retained as a consistency or error check. The solution of Equation (15) is compared to the pressure determined at each state evaluation with the density and temperature resulting from Equations (11) through (14).

The liquid entropy is also calculated with each state evaluation. The purpose is yet another consistency check. During the interval (τ_1, τ_3) when there is no flashing, the blowdown is isentropic. After τ_3, the liquid entropy decreases as the liquid system is cooled. Confirmation of this provides a check on the correctness of the formulation and the accuracy of the integration.

The system (11) through (15) gives the response of the bulk liquid. It is recognized that at the loss of some rigor, Equations (13) through (15) can be replaced by

$$\frac{dP}{d\tau} = a^2 \frac{d\rho}{d\tau} \tag{16}$$

if the liquid process is assumed isentropic. Because of the conveniences afforded by both the automatic solver (described below) and the Keenan-based property package [18], there is no compelling incentive to simplify the system. The full system provides rigor and internal accuracy checks. It also obviates the need to generate a fit for the adiabatic compressibility (appearing in Equation (16)) as a function of pressure and initial entropy. For the PWR conditions postulated here, the adiabatic compressibility varies by 10% or more over the anticipated pressure range. For production calculations, the simplification afforded by Equation (16) would be weighed more carefully.

Solution Technique

Generally available mathematical software has been used to solve the coupled systems of equations that include the microscopic flashing model, Equation (7) and (8), and the macroscopic liquid state, Equation (11) to (15). The first step in the solution consists of transforming the mixed system of partial and ordinary differential equations to a larger system containing only ordinary differential equations. The resulting system of equations is then integrated in time using an automatic ordinary differential equation solver.

A method-of-lines technique [19] is used to convert the bubble thermal layer energy equation, Equation (8), into a system of ordinary differential equations. This consists of replacing all spatial derivatives appearing in the partial differential equation by suitable finite-difference approximations. Specifically, this replacement is performed using the PDEONE software

interface [20]. This interface uses novel three-point central differences to approximate the spatial derivatives. The reader is referred to [20] for the somewhat lengthy details. The resulting system of ordinary differential equations is tri-diagonal. That is, the expression for the temperature derivative at the ith spatial node, $d\theta_i/d_\tau$ involves only θ_{i-1}, θ_i, and θ_{i+1}. However, the banded nature of this subsystem is destroyed when the bubble motion equation and the macroscopic field equations are attached.

The second step in the solution consists of integrating the resulting system of ordinary differential equations (ODE) in time. The automatic ODE solver described in [21] has been used to integrate the coupled system of equations.

Although automatic software like that used in the present study appears not to have received widespread attention in the engineering literature (see [19] for notable exceptions, however), its use offers several significant advantages. Some advantages of the solver used here are:

1. The ODE solver automatically adjusts both time-step size and order of integration to accommodate specific problem characteristics. The solution is obtained efficiently, subject to a specified local error tolerance. This obviates the need to perform extensive time-step convergence studies.

2. The ODE solver allows the use of either non-stiff Adams-type methods (generalizations of the trapezoidal rule) or stiffly stable backward differentiation methods (generalization of the backward Euler rule. It is possible to specify externally the manner in which the associated non-linear corrector equations will be solved. For example, the non-stiff methods are used to predict the highly active transient following nucleation in the Friz et al. experiment [4]. Stiff methods using a Newton-like chord iteration are switched on later to predict the relatively gradual pressure recovery. It is emphasized that this machinery is conveniently available (see [21, 24]) and does not require extensive re-programming and analysis of well-established methods.

3. The ODE solver uses sparse matrix techniques, and thus it is possible to obtain an economical solution for unbanded but sparse problems like the present one. Note that the bubble motion equation and the macroscopic field equations destroy the band structure of discretized thermal layer equation.

4. The ODE solver possesses several non-standard capabilities that were used in the prediction of the Friz, et al chamber-piston experiment. As will be described later, a parametric study has been performed to determine the effect of nucleation superheat on pressure response. A nominal superheat is prescribed and the pressure at which bulk nucleation will actually occur is calculated from the Clayeron expression. The ODE solver has both extrapolatory and interpolatory algebraic root-finders that are directly coupled to the time integrator. This feature has been used to automatically determine the time τ_3 when bulk nucleation occurs. At this time, the branches of Equations (11) to (13) for $\tau > \tau_3$ are switched on and the microscopic flashing model is also turned on. The direct coupling of algebraic root-finders with the time integrator also allows the efficient negotiation of otherwise troublesome discontinuities in the first derivative. The lack of this capability in many high quality ODE solvers is one of the major reasons the use of such software is not more widespread in the engineering community.

5. One advantage of the ODE solver that cannot be over-emphasized is the fact that it permits and facilitates the simultaneous solution of the complete set of defining equations. Therefore, it is not necessary to use unnecessarily restrictive physical assumptions in order to de-couple the various sub systems of equations.

6. The modular nature of the automatic software used here allows the defining equations to be programmed in a relatively straightforward and natural manner. It is possible to clearly separate the problem to be solved, the mathematicl model of that problem, and the numerical technique used to approximate a solution of the problem. This frees the engineer to concentrate on the physical aspects of the problem and not the mathematical and programming aspects. The modularity also enhances the quality of the analysis.

RESULTS

The formulation and solution of the microscopic flashing model, Equations (7) and (8), are checked by predicting bubble growth for two cases in which the pressure field is prescribed. Pressure-recovery predictions for the Friz, et al. chamber-and-piston experiment are then presented for combinations of the two input parameters, nucleation superheat and nucleation density.

Bubble Growth in Constant-Pressure Water

Calculated bubble growth in low pressure water at constant pressure is shown in figure 1, in which the bubble surface velocity is plotted against the instantaneous bubble radius. The result from the microscopic flashing model is compared with the Rayleigh and Plesset-Sqick solutions:

$$\frac{dr_b}{d\tau} = \frac{R_{bo}}{\tau} \frac{2}{3} \left[\frac{P_s(T_\infty) - P}{\rho_f} \right] \qquad \text{(Rayleigh)}$$

$$\frac{dr_b}{d} = \frac{6}{\pi} Ja^2 r_b^{-1} \qquad \text{(Plesset-Zwick)}$$

Figure 1 shows that the microscopic flashing model correctly predicts the transition from the inertia to the conduction-controlled region of growth.

The thermal boundary layer for this case is plotted against time in Figure 2. The bubble surface is located at y=0, and the boundary condition corresponding to Equation (9d) is imposed at y=4. Note that the interface temperature drops rapidly as bubble growth passes almost immediately from the inertia to the conduction-limited region. The interface temperature $(0, \tau)$ asymptotically approaches 1 as it should. The very fine spatial net for the y-interval (0,4) evident in Figure 2 is used only to demonstrate the smoothness and accuracy of the solution technique. Convergence studies

have been performed with the result that bubble radius can be predicted to three significant digits with fewer than 12 spatial nodes.

Bubble Growth in Decompressing Water

Niino [6,7] has measured bubble growth in decompressing water. In this experiment, the liquid pressure was allowed to decay until the liquid became sufficiently superheated. A bubble was caused to grow by pulsing a laser through the liquid. Subsequent growth was recorded by photographic means.

The data from Figure 67 of Niino'sthesis is plotted in Figure 3 along with results of the present analysis and of the constant superheat theory. The dashed lines are Niino's estimation of the scatter in the bubble diameter data. The solid curves represent results obtained from Equations (7) and (8) assuming a linear pressure decay (-8.78×10^{-3} MPa/ms, which is mild compared to postulated PWR blowdown rates) and two different initial pressures. The lower curve is obtained with the initial pressure of 0.183 MPa recorded by Niino. This corresponds to an initial superheat of 1.05 K. The curve falls slightly below the bubble diameter data. The higher curve is obtained with an initial pressure of 0.180 MPa, which gives an initial superheat of 1.56 K. This curve passes through the data.

Niino does not provide the experimental uncertainties for the liquid pressure and temperature measurements. Certainly a 3 kPa discrepancy in initial pressure (i.e., a shift in the pressure trace 0.3 ms to the left) could result from instrument error and synchronization error. Therefore the analysis is judged to be in excellent agreement with the data. The constant superheat theory on the other hand significantly underpredicts bubble growth.

Bubble Growth and Pressure Recovery with a Prescribed Strain

The chamber-and-piston experiment of Friz, et al. [4] provides an opportunity to assess the capabilities of the present analysis and to study the

significance of two parameters, nucleation superheat and nucleation density. The Friz experimental apparatus is a closed system of initially subcooled, high pressure water contained within a spherical chamber (14 cm in diameter) connected to a piston. Piston displacement is caused by reducing the nitrogen back pressure on the piston. The measured data includes liquid temperature, liquid pressure, and piston displacement.

The Figure 2 data of [4] are reproduced in Figure 4 along with two analytical results. Note that the liquid temperature is in the range of PWR operation. The blowdown rate (0.1 MPa/ms) is only an order of magnitude smaller than values postulated for a loss-of-coolant accident. Also note that pressure recovery occurs simultaneously with the arrest of piston motion.

The question is this: did bulk nucleation occur at the time when the piston motion was arrested? Was bulk nucleation in fact caused by mechanical disturbances resulting from piston arrest? Or did bulk nucleation occur as early in the transient as the time when the saturation pressure was reached? That is, could it be that the internal compressive strain exerted by the bubbles on the liquid was simply insufficient to overcome the externally imposed expansive strain until the time when piston motion was arrested? The question is important, because transient pressure data like these and Lienhard's [5] are used to infer the superheat at which bulk nucleation happens. The point is that the mechanics of the blowdown may have to be taken into account before inferences regarding bulk nucleation are drawn from pressure-time data alone. Thus, the analytical capability presented here can be of help in inferring the onset of bulk nucleation from pressure-time data.

Unfortunately, the piston and displacement data shown in Figure 4 were found to be inconsistent. During the subcooled portion of the transient, the change in pressure from its initial value is known to be very nearly a linear function of piston displacement:

$$\Delta P = -\rho a^2 \frac{\Delta V}{V_1} \qquad (17)$$

Such a linear relationship between the measured data is not apparent. Another inconsistency concerns the final or total piston displacement, which is not reported in [4]. A value of $\Delta V/V_1 = 2.8 \times 10^{-3}$ is reported in Figure 15 of [25]. However, this value is not large enough to permit the system to expand to 7.74 MPa, the minimum pressure of Figure 4. This conclusion is based on hand calculations in which the thermodynamic properties appearing in the above expression have been evaluated with the STP package [18]. The sound speed calculation of the STP package has been verified with experimental sound speed data in the compressed and saturated liquid range.

Because of the inconsistency in the data, the reported displacement curve was ignored. A new displacement curve was inferred from the measured pressure data. In other words, the question of when bulk nucleation occurs has been begged. It is implicitly assumed in the generation of the new displacement curve that bulk nucleation does not occur until piston motion is arrested. This is disappointing. Nevertheless, the calculations discussed below do indicate that early nucleation before pressure recovery is indeed possible.

The solid curve plotted in Figure 4 is the best fit of the present analysis to the pressure data. It has been obtained with the assumption that bulk nucleation occurs at 10^9 sites/m^3 when the liquid superheat reaches a nominal value of 7.8 K. Again, the agreement between the analysis and the pressure data before "turn-around" is excellent, because the new displacement curve was generated to make it so.

The dashed curve in Figure 4 has been obtained with the present analysis assuming $N = 5.6 \times 10^9$ sites/m^3 and $\Delta T = 0.01$ K. These are the values used by Friz, et al. to obtain their best analytical fit to the data, which in fact passes through the pressure data. Friz, et al. assume that bulk nucleation occurs immediately upon the liquid reaching saturation($\Delta T=0$), and they use the Plesset-Zwick formula to calculate flashing. The instantaneous value of superheat is substituted into the Plesset-Zwick formula. The difference between the dashed curve of Figure 4 and the Friz, et al. analysis may be

indicative simply of differences in the displacement curves used. The discrepancy however most likely confirms that constant superheat theory is inadequate for predicting flashing in rapid pressure transients.

Two other observations may be made regarding the dashed curve of Figure 4. Note that because of the large nucleation site density assumed, pressure "turn-around" occurs before piston motion is arrested. Also the maximum predicted liquid superheat is not the superheat at which bulk nucleation is triggered.

Figures 5 and 6 provide additional information regarding the "best-fit" solution obtained with a nominal nucleation superheat of 7.8 K and nucleation density of 10^9 sites/m^3. The interface temperature appears to be asymptotically approaching the saturation temperature that corresponds to the initial entropy. Note in Figure 6 that the temperature defect remains finite even as the liquid superheat vanishes asymptotically.

It should be mentioned that the thermal boundary layer is not thin relative to the instantaneous value of the bubble radius. Almost immediately after nucleation, the ratio of thermal-layer thickness to radius is 1.3. At 100 ms, the ratio is 1.9.

Figure 6 also reveals that bubble growth rapidly passes into the conduction-limited region after nucleation occurs. As the pressure recovers, bubble growth seems to pass back into the inertia-controlled domain. Since the liquid superheat is vanishing, it makes little computational difference whether bubble growth is inertia or conduction limited. As Figure 5 shows, bubble growth has virtually stopped when this happens. However, the unexpected passage back into the inertia-controlled growth region may be unrealistic. In the course of the parametric studies, the temperature defect at the bubble surface was observed to approach either 0 or 1 depending on the value of the bubble density N.

This possible anomaly is not caused by the algorithm. However, it may indicate that the particular choice of N and ΔT is not valid, even though the choice produces a good fit to the pressure data. The suspected anomaly brings into question the validity of the assumption used in generating the new

displacement curve: bulk nucleation occurs at the maximum liquid superheat. Unfortunately, resolution of the question hinges on knowing the true piston displacement curve.

The results of the "best-fit" analysis are otherwise reasonable. A void fraction may be calculated from the bubble radius data provided in Figure 5. The void asymptotically approaches a value of 0.002. Thus the assumption that the uniformly dispersed bubbles grow independently without interference is not violated.

Results of the parametric study obtained by varying the nucleation superheat and the nucleation density are provided in Figures 7 and 8. The dashed curve of Figure 7 has been generated with 10^9 sites/m^3, the same value used in the "best-fit" analysis. However, bulk nucleation is caused to occur in this case almost immediately after the liquid becomes superheated. Note that the pressure "turn-around" is quite sharp and occurs simultaneously with piston arrest. Again, the point of minimum pressure or maximum liquid superheat is not predicted to occur with the onset of bulk nucleation.

The calculations shown in Figure 8 are done with the nominal nucleation superheat set to 7.8 K, the "best-fit" value. The experimental pressure data are bounded above by the calculation with 10^{10} sites/m^3 and below by the calculation with 10^8 sites/m^3. Interestingly, the thermal layer profile for 10^{10} sites/m^3 looks very much like Figure 6, the "best-fit" profile. The thermal layer profile for the 10^8 sites/m^3 looks like the profile of Figure 2. That is, for large values of N, the bubbles appear to pass into and out of the conduction-limited region of growth. For small values of N, the bubbles pass from the inertia-limited region and remain in the conduction-limited region of growth. This latter behavior, as mentioned earlier, is intuitively more acceptable.

A calculation with 10^8 sites/m^3 and a nominal nucleation superheat of 0.01 K has been made. The results look very much like the 10^8 sites/m^3 curve of Figure 8. That is, the calculation bounds the experimental pressure data from below. Thus the data is bounded from above (see Figure 7) and

and below by calculations using the input pairs (0.01 K, 10^9 sites/m^3) and (0.01 K, 10^8 sites/m^3). This suggests there may be an intermediate value of nucleation density that fits the data as well as the "best-fit" calculation.

The pressure recovery of Figure 9 was calculated with a nominal superheat of 0.01 K and a nucleation density of 5 x 10^8 sites/m^3. Indeed, it appears that an intermediate value of nucleation density can be found that will fit the data nearly as well as the "best-fit" calculation. The thermal layer profile corresponding to the prediction shown in Figure 9 has the appearance of the profile of Figure 2. That is, the bubbles pass from the inertia-limited region and remain in the couduction-limited region of growth.

SUMMARY AND CONCLUSIONS

A detailed, microscopic model for the nonequilibrium flashing of water has been coupled to equations describing the bulk liquid state. The pressure response of the liquid has been calculated for a prescribed external liquid strain. The effect of nucleation superheat and nucleation density on predicted pressure response has been studied.

The flashing model is predicated on the dynamics of a single bubble growing in an infinite liquid. The model involves the solution of a system of ordinary and partial differential equations that constitute a classic moving-boundary problem. The problem is made stationary by a transformation of variable. The solution is obtained numerically by the method of lines and by the use of automatic software.

The power and convenience provided by the software has made it possible to retain physical detail and rigor in the analysis. Thus the flashing model encompasses both the inertia and conduction-limited regions of bubble growth. The analysis is applicable at the high temperatures of PWR operation. The solution is not limited by the assumption of a thin thermal boundary layer or by a prescribed boundary layer shape. The model can handle arbitrary pressure transients, both decompressive and recompressive. The rigor employed in describing the bulk liquid state permits redundant accuracy checks.

The correctness of the formulation and solution has been demonstrated by analyzing two bubble-growth problems in which the liquid pressure is prescribed. For the constant-pressure case, the analysis correctly predicts the transition from inertia to conduction-limited growth. The analysis is also in excellent agreement with the measurements of bubble growth in decompressing water made by Niino.

The chamber-and-piston experiment of Friz, et al. has been analyzed. The pressure response of the system has been studied for various combinations of the two input parameters, nucleation superheat and nucleation density.

The results of the parametric study are not definitive, because of uncertainties and apparent inconsistencies in the experimental pressure and piston displacement data. Nevertheless, the analytical results are interesting in themselves, and some conclusions can be reached more or less independently of the data.

A "best-fit" has been obtained to the Friz, et al. data with a nominal superheat of 7.8 K and bubble density of 10^9 sites/m^3. In the "best-fit" calculation, bulk nucleation is triggered upon reaching the maximum experimentally observed liquid superheat. The plot of the bubble thermal layer for this case indicates that bubble growth quickly passes from the inertia to the conduction limited region. However, as recovery proceeds toward an equilibrium end state, the bubble appears to pass back into the inertia-limited region. This behavior is intuitively judged to be unrealistic. This seemingly anomolous behavior is not thought to be computational or numerical in nature as it has been shown to be a function of the nucleation density.

It appears that more than one combination of nucleation superheat and nucleation density can produce an adequate fit to the Friz, et al. pressure data. In addition to the "best-fit", the data can also be reasonably predicted with a very small value of nucleation superheat. Although the pressure predictions for these calculations are similar, the predicted responses of the bubble thermal layer are not. In one case (large nucleation superheat and density), recovery proceeds toward equilibrium with bubble growth limited by liquid inertia; in the other (small nucleation and density superheat), by conduction through the bubble thermal layer. The latter behavior appears more reasonable.

The results of the parametric studies summarized in Figures 7, 8 and 9 underscore the difficulty of inferring the onset of bulk nucleation from pressure-time data alone. It is demonstrated analytically that bulk nucleation can occur long before the minimum pressure or, euqivalently, the maximum liquid superheat is attained. The mechanics of bhe blowdown process must be taken into account. Pressure "turn-around" occurs when the compressive strain induced by bubble growth balances and then overcomes the externally imposed strain. The parametric studies also confirm that constant superheat theory does not adequately predict nonequilibrium flashing in praid pressure transients.

Although scant attention has been given here to the execution statistics of the analysis, it does appear feasible to extend the method to a Lagrangian description of the liquid. This next step will permit the incorporation of nonequlilibrium flashing into the calculation of wave action in the ruptured piping of a PWR following a design basis accident.

REFERENCES

1. A. R. Edwards and T. P. O'Brien, "Studies of Phenomena Connected with the Depressurization of Water Reactors," Journal of the British Nuclear Energy Society, Vol. 9, April 1970, pp 125-135.

2. G. F. Brockett, H. D. Curet, H. W. Heiselmann, Experimental Investigations of Reactor System Blowdowns, IN-1348, Idaho Nuclear Corporation, September 1970.

3. R. Allemann et al., Experimental High Enthalpy Water Blowdown from a Simple Vessel Through a Bottom Outlet, BNWL-1411 UC80, Battelle Memorial Inst., 1980.

4. G. Friz, W. Riebold, W. Schulze, "Studies on Thermodynamic Nonequilibrium in Flashing Water," Specialists Meeting on Transient Two-Phase Flow, OECD Nuclear Energy Agency, Toronto, August 1976.

5. J. H. Lienhard, Md. Alamgir, M. Trela, "Early Response of Hot Water to Sudden Release from High Pressure," ASME Journal of Heat Transfer, Vol. 100, August 1978, pp 473-479.

6. M. Niino, Study of Single Bubble Generation and Growth by Laser Beam, Ph.D. Thesis, University of Tokoku, Japan, 1975 (in Japanese).

7. O. C. Jones, Private Communication: Transmittal of Niino Thesis in Part, November 14, 1978.

8. J. H. Keenan, F. G. Keyes, P. G. Hill, J. G. Moore, Steam Tables: Thermodynamic Properties of Water, New York; John Wiley and Sons, 1969.

9. W. H. Besant, Hydrostatics and Hydrodynamics, Cambridge, 1859.

10. Lord Rayleigh, "On the Pressure Developed in a Liquid During the Collapse of a Spherical Cavity," Philos. Mag., Vol. 34, 1917, pp 94-98.

11. M. S. Plesset and S. A. Zwick, "The Growth of Bubbles in Superheated Liquids", Journal Appl. Phys., Vol. 25, April 1954, pp 493-500.

12. H. K. Forster and N. Zuber, "Growth of a Vapor Bubble in a Superheated Liquid", Journal Appl. Phys., Vol 25, 1954, pp 474-478.

REFERENCES (Continued)

13. L. E. Scriven, "On the Dynamics of Phase Growth," Chem. Eng. Sci., Vol. 10, 1959, pp 113.

14. B. B. Mikic, W. M. Rohsenow, and P. Griffith, "On Bubble Growth Rates," Int. J. Heat Mass Transfer, Vol. 13, 1970, pp 657-666.

15. O. C. Jones and N. Zuber, "Bubble Growth in Variable Pressure Fields," ASME J. Heat Transfer, Vol. 100, 1978, pp 453-459.

16. T. Theofanous, L. Biasi, H. S. Isbin, and H. Fauske, "A Theoretical Study on Bubble Growth in Constant and Time-Dependent Pressure Fields," Chem. Eng. Sci., Vol. 24, 1969, pp 885-897.

17. W. J. Bornhorst and G. N. Hatsopoulos, "Bubble-Growth Calculation Without Neglect of Interfacial Discontinuities," ASME J. Appl. Mech., Vol. 34, 1967, pp 847-853.

18. F. Aguilar, P. G. Tuttle, and A. H. Meadows, "STP: Fortran Library for Steam Table Properties," NPGD-TM-514, 1979, Babcock & Wilcox, Co., Lynchburg, VA.

19. N. B. Carver, "Method of Lines Solution of Partial Differential Equations: Some Standard and Devious Applications," Computational Methods in Nuclear Engineering Proceedings of the 1979 American Nuclear Society Topical Meeting, Williamsburg, VA., pp 8.54-8.75.

20. R. F. Sincovec and N. K. Madsen, "Software for Nonlinear Partial Differential Equations," ACM Transactions on Mathematical Software, Vol. 1, No. 3, 1975, pp 232-260.

21. S. Thompson and P. G. Tuttle, DSTPGT: Automatic Software for the Numerical Solution of Differential Equations - Test and Certification Report, NPGD-TM-521, Babcock & Wilcox, Co., January 1980.

22. A. C. Hindmarsh, "GEAR: Ordinary Differential Equation System Solver," UCID-30001 (Rev. 3), Lawrence Livermore Laboratory, Livermore, CA., December 1974.

23. A. C. Hindmarsh, "A Collection of Software for Ordinary Differential Equations," Computational Methods in Nuclear Engineering Proceedings of the 1979 American Nuclear Society Topical Meeting, Williamsburg, VA., April 1979, pp 8.2-8.15

24. J. W. Spellman and A. C. Hindmarsh, GEARS: Solution of Ordinary Differential Equations having a Sparse Jacobian Matrix, UCID-30130, Lawrence Livermore Laboratory, August 1975.

25. K. Wolfert, "The Simulation of Blowdown Processes with Consideration of Thermodynamic Nonequilibrium Phenomena," Specialists Meeting on Transient Two-Phase Flow, OECD Nuclear Energy Agency, Toronto, August 1976.

FIGURES AND CAPTIONS

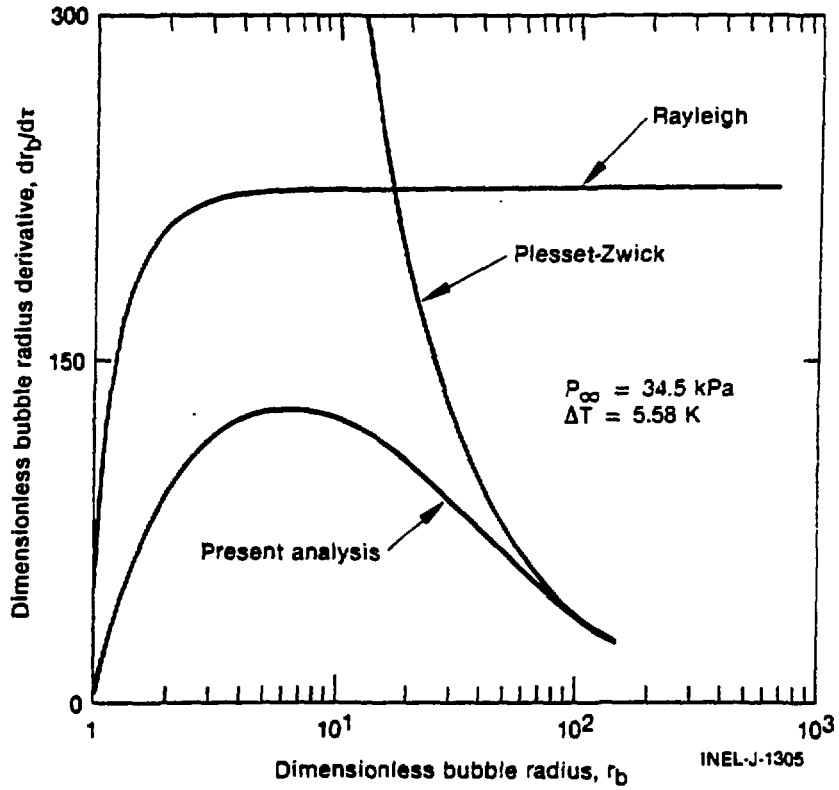
300
150
0
1
10^1
10^2
10^3
Dimensionless bubble radius derivative, $dr_b/d\tau$
Dimensionless bubble radius, r_b
Rayleigh
Plesset-Zwick
Present analysis
P_∞ = 34.5 kPa
ΔT = 5.58 K
INEL-J-1305

Figure 1

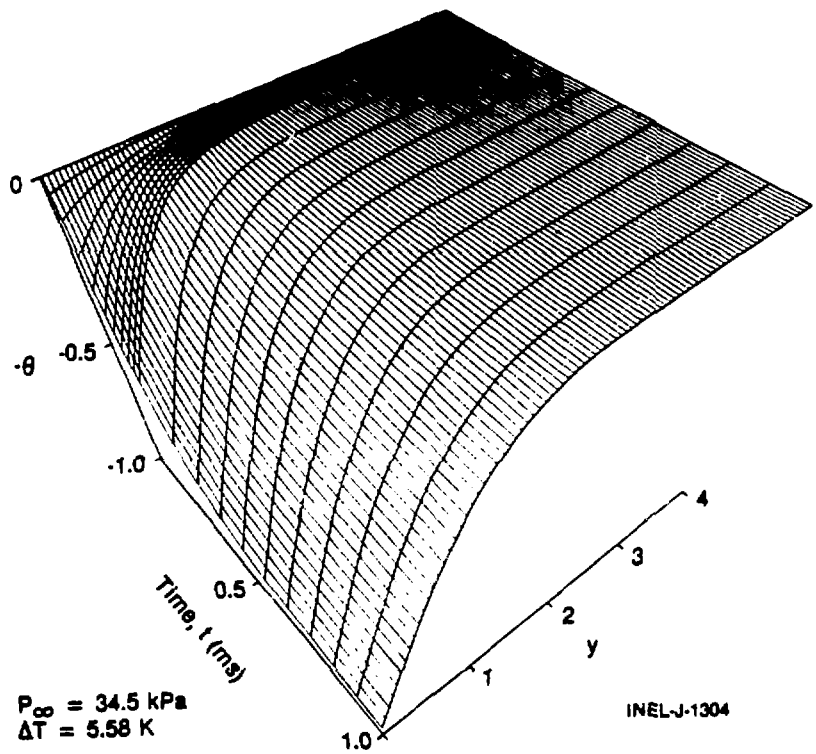

Figure 2

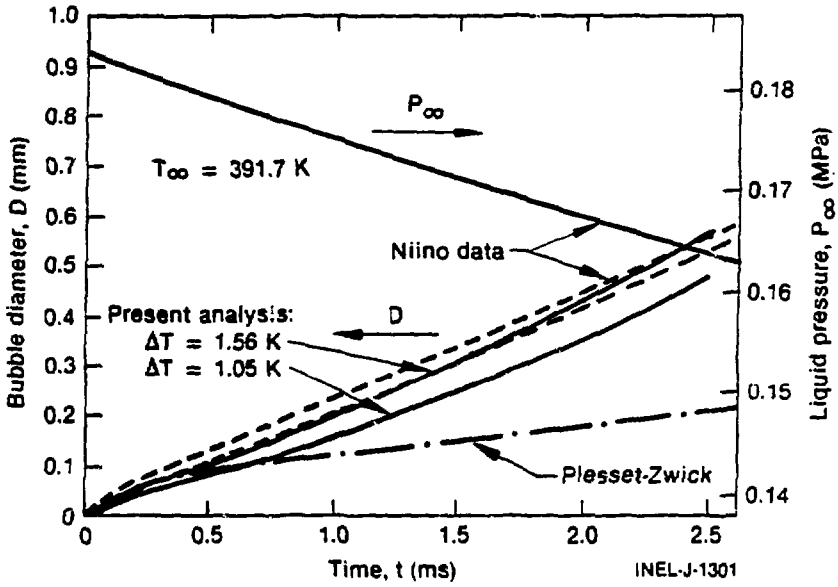
Bubble diameter, D (mm)
Liquid pressure, P_∞ (MPa)
Time, t (ms)
P_∞
T_∞ = 391.7 K
Niino data
Present analysis:
ΔT = 1.56 K
ΔT = 1.05 K
D
Plesset-Zwick
INEL-J-1301

Figure 3

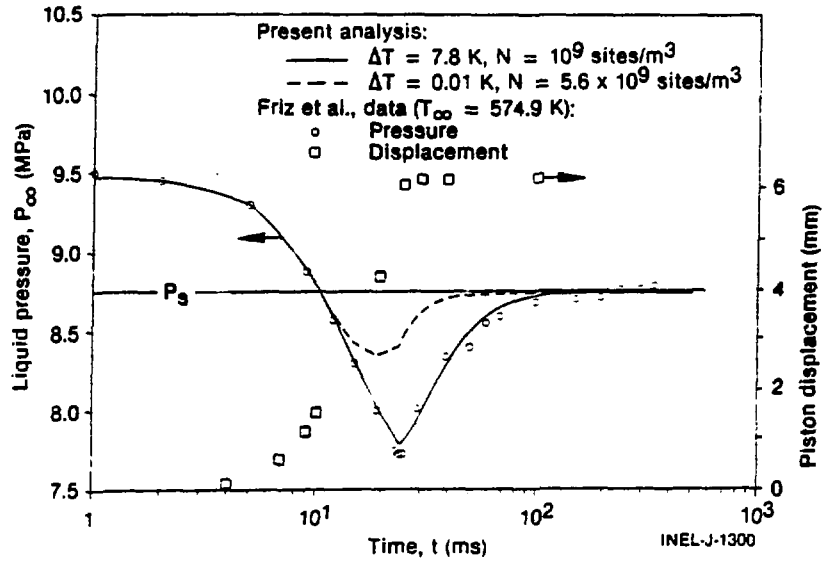

Figure 4

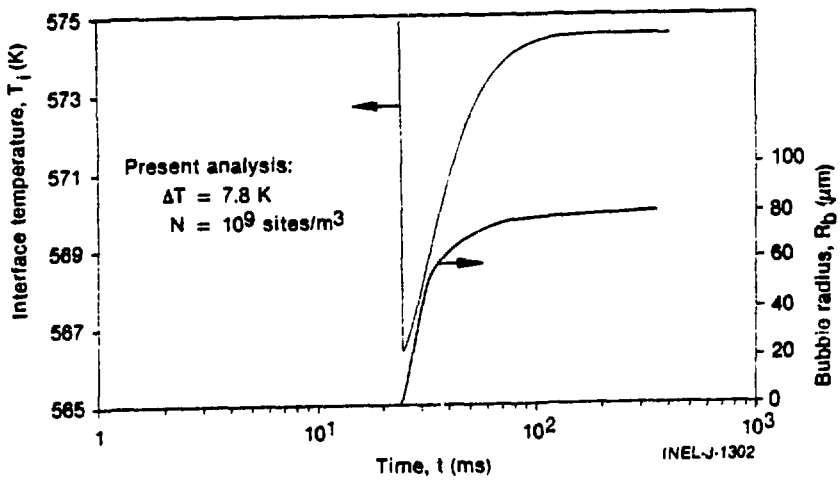

Figure 5

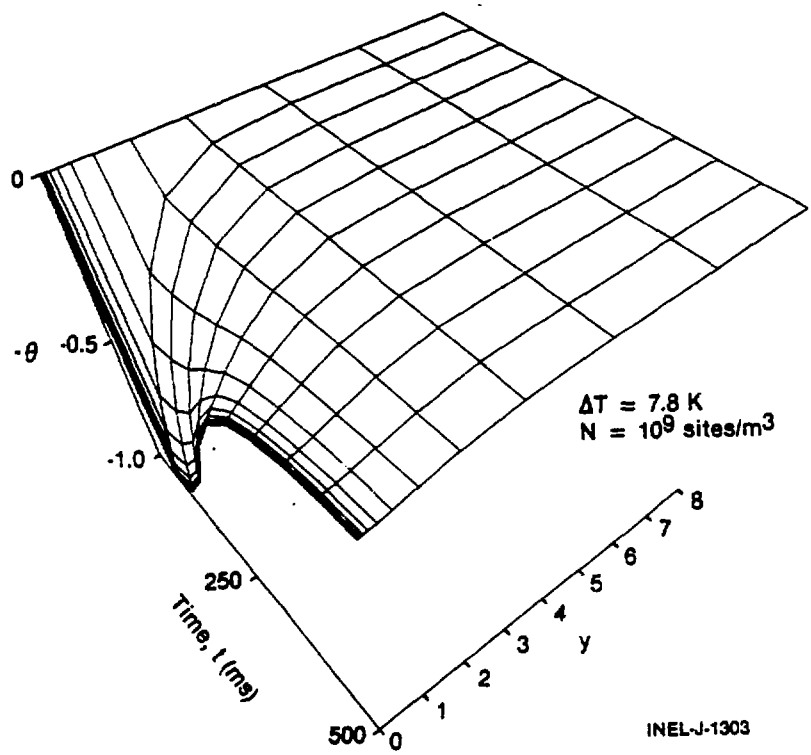
0
-θ
-0.5
-1.0
ΔT = 7.8 K
N = 10^9 sites/m^3
250
Time, t (ms)
500
0
1
2
3
4
5
6
7
8
y
INEL-J-1303

Figure 6

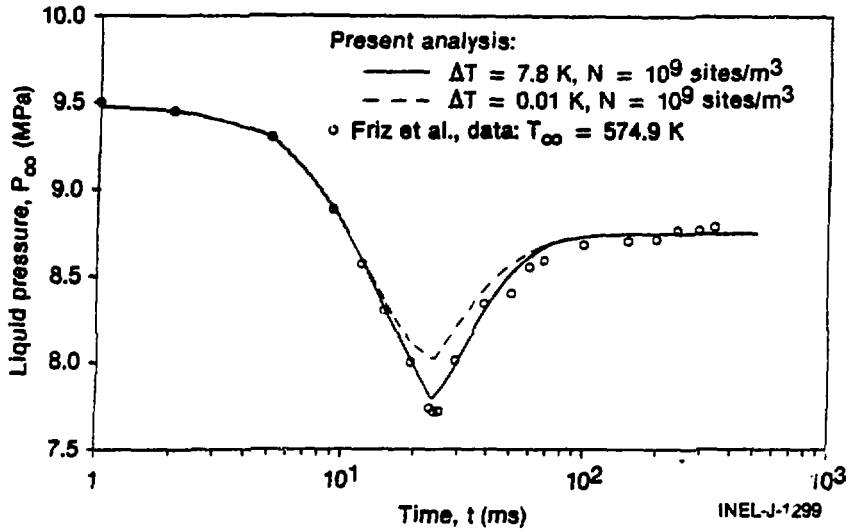

Figure 7

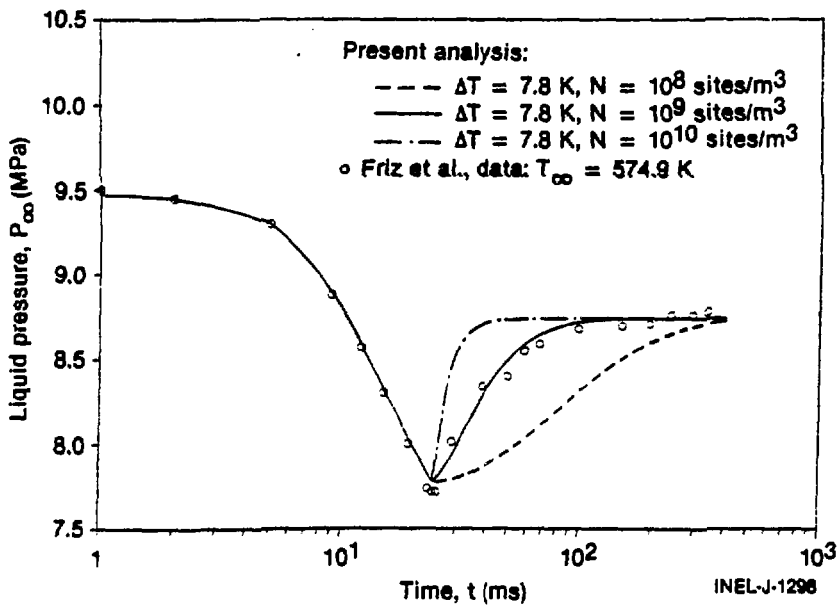

Figure 8

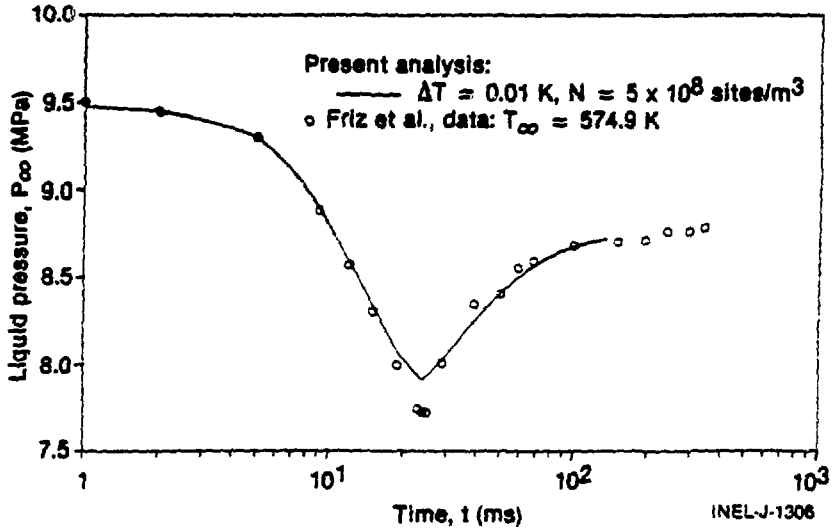
Present analysis:
ΔT = 0.01 K, N = 5 x 10^8 sites/m^3
Friz et al., data: T∞ = 574.9 K
Liquid pressure, P∞ (MPa)
10.0
9.5
9.0
8.5
8.0
7.5
1
10^1
10^2
10^3
Time, t (ms)
INEL-J-1306

Figure 9